Role of the Oxide Support on the Structural and Chemical Evolution of Fe Catalysts during the Hydrogenation of CO_2

Mauricio Lopez Luna, Janis Timoshenko, David Kordus, Clara Rettenmaier, See Wee Chee, Adam S. Hoffman, Simon R. Bare, Shamil Shaikhutdinov,* and Beatriz Roldan Cuenya

Read Online

ACCESS | Metrics & More | Article Recommendations | Supporting Information

ABSTRACT: Iron-based catalysts are considered active for the hydrogenation of CO_2 toward high-order hydrocarbons. Here, we address the structural and chemical evolution of oxide-supported iron nanoparticles (NPs) during the activation stages and during the CO_2 hydrogenation reaction. Fe NPs were deposited onto planar SiO_2 and Al_2O_3 substrates by dip coating with a colloidal NP precursor and by physical vapor deposition of Fe. These model catalysts were studied *in situ* by near-ambient pressure X-ray photoelectron spectroscopy (NAP-XPS) in pure O_2, then in H_2, and finally in the $CO_2 + H_2$ (1:3) reaction mixture in the mbar pressure range and at elevated temperatures. The NAP-XPS results revealed the preferential formation of Fe(III)- and Fe(II)-containing surface oxides under reaction conditions, independently of the initial degree of iron reduction prior to the reaction, suggesting that CO_2 behaves as an oxidizing agent even in excess of hydrogen. The formation of the iron carbide phase, often reported for unsupported Fe catalysts in this reaction, was never observed in our systems, even on the samples exposed to industrially relevant pressure and temperature (*e.g.*, 10 bar of $CO_2 + H_2$, 300 °C). Moreover, the same behavior is observed for Fe NPs deposited on nanocrystalline silica and alumina powder supports, which were monitored *in situ* by X-ray absorption spectroscopy (XAS). Our findings are assigned to the nanometer size of the Fe particles, which undergo strong interaction with the oxide support. The combined XPS and XAS results suggest that a core (metal-rich)−shell (oxide-rich) structure is formed within the Fe NPs during the CO_2 hydrogenation reaction. The results highlight the important role played by the oxide support in the final structure and composition of nanosized catalysts.

KEYWORDS: iron catalysts, CO_2 hydrogenation, X-ray photoelectron spectroscopy, X-ray absorption spectroscopy
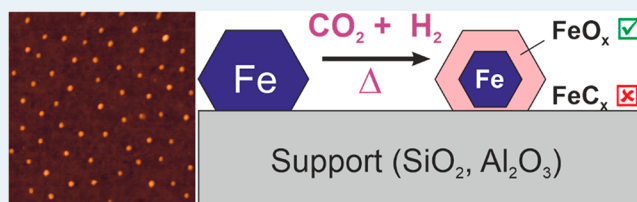
1. INTRODUCTION

Due to ecological and global climate concerns, there is a growing interest in developing environmentally friendly technologies to utilize CO_2, especially in applications where it is reacted with H_2 (which can be obtained from renewable sources) to produce value-added chemical products such as high-order hydrocarbons and alcohols.[1,2] In this respect, one approach that has received considerable attention is the so-called "modified" Fischer−Tropsch (FT) synthesis (or CO_2−FTS), which uses CO_2 as a feedstock instead of CO. The concept is to combine the reverse water−gas shift (r-WGS) reaction (*i.e.*, $CO_2 + H_2 \rightarrow CO + H_2O$) and the subsequent hydrogenation of syngas (CO + H_2) via the classical FT process on a single catalyst. Since Fe-based catalysts were found active for both reactions, iron has become the most studied component of the CO_2−FTS catalysts. To improve both the activity and selectivity toward C_{2+} products, iron is usually promoted by other 3d metals like Co, Ni, Cu,[3,4] or alkali metals like K and Na.[5−7]

It is not surprising that many ideas about CO_2 hydrogenation catalysts on Fe originate from the more studied FTS systems, where the active phase is commonly associated with Fe carbides, in particular Hägg carbide (χ-Fe_5C_2), probably coexisting with the Fe oxide phase.[8−12] Iron carbides are also frequently considered to be the active phase(s) for CO_2 hydrogenation, with the reduced state of iron playing an essential role for the carbide formation.[13] For example, a comparative study of CO_2−FTS catalysts prepared from Fe_2O_3 and $CuFeO_2$ and activated in H_2 revealed a greater extent of the Fe(III) → Fe(0) reduction in $CuFeO_2$, that favored the selective carburization toward the Hägg carbide and improved the selectivity toward higher (C_{5+}) hydrocarbons considerably.[4] Direct conversion of CO_2 to gasoline-range (C_5−C_{11}) hydrocarbons was demonstrated on a multifunctional catalyst (Na−Fe_3O_4/HZSM-5), which cooperatively catalyzed a tandem reaction, presumably on three types of active sites (Fe_3O_4, Fe_5C_2, and acid sites in zeolite).[14] Recently, the
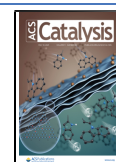
structural evolution of the bulk iron-containing phases in CO_2 hydrogenation was established under reaction conditions using a combination of Raman spectroscopy and X-ray diffraction coupled with online gas chromatography.[15] During the activation in pure hydrogen and the subsequent CO_2 hydrogenation reaction, the iron oxides (α-Fe_2O_3 and γ-Fe_2O_3) underwent the following transformation: α-Fe_2O_3 (γ-Fe_2O_3) → α-Fe_3O_4 (γ-Fe_3O_4) → α-Fe (γ-Fe) → χ-Fe_5C_2 (θ-Fe_3C). Both iron carbide phases showed high catalytic activities, with χ-Fe_5C_2 exhibiting highest selectivity toward lower olefins.

Although the Fe-based CO_2−FTS catalysts are often used unsupported, it has been documented that the support can influence the catalytic performance as a result of its effect on the reduction and carburization. For example, the activity of Fe/SiO_2 catalysts was found to be substantially lower than Fe/C catalysts.[16] It was hypothesized that a stronger interaction of the iron oxide with the silica inhibited the reduction to the active metallic iron. Additionally, mixing silica and iron oxide resulted in a nonlinear dependence of the catalytic activity and selectivity in the FT reaction as a function of the Fe/Si ratio.[17] The complexity of NP/support interactions has been addressed in several review articles; see, for example, ref 18. The support may affect the initial dispersion of the Fe nanoparticles (NPs) and the possible agglomeration during the reaction that may, in turn, influence the catalytic performance.[19] Considerable particle size effects have recently been reported for ZrO_2-supported Fe catalysts,[20] as well as for SiO_2-supported Ni NPs,[21] but a systematic study of particle size effects for C_{2+} production is still missing.

Despite significant progress in recent years, further work is still needed to elucidate the reaction mechanism. This would allow the rational design of more efficient and selective CO_2−FTS catalysts. In this respect, fundamental studies applying surface-sensitive techniques to well-defined model systems may substantially contribute to a deeper understanding of the relationship between reactivity and structural/chemical parameters of the real catalysts. Although such "surface science" studies are usually carried out in ultrahigh vacuum (UHV) conditions, modern advances of surface science techniques such as near-ambient pressure X-ray photoelectron spectroscopy (NAP-XPS) provide the possibility of studying catalytic systems under more realistic conditions.[22−25]

In order to shed light on the state of Fe under CO_2 hydrogenation reaction conditions and the role of the support in the structural and chemical evolution of the Fe-based catalysts, in this work, we performed NAP-XPS studies of several model systems prepared on planar SiO_2 and Al_2O_3 supports. Fe NPs were synthesized using an inverse micelle encapsulation method that allows the fabrication of mono-dispersed NPs.[26,27] In addition, we used physical vapor deposition (PVD) of Fe to mimic fully reduced, metallic NPs. To model supported powder catalysts, micellar NP precursors were deposited onto nanocrystalline SiO_2 and Al_2O_3 powder supports and studied in situ by NAP-XPS and X-ray absorption spectroscopy (XAS) in different gas atmospheres. The XAS results revealed a high stability of the iron oxide phases under reaction conditions and considerable amounts of metallic iron in the catalysts. The combined XPS and XAS results indicate the formation of a core (metal-rich)−shell (oxide-rich) NP structure. Moreover, in contrast to previously reported studies on Fe-based catalysts, iron carbide phases were not observed in any of our model catalysts studied,

revealing the crucial role of the support on the structural evolution of highly dispersed Fe catalysts.

2. METHODS AND MATERIALS

Iron NPs were synthesized by the inverse micelle encapsulation method.[28] A solution using poly(styrene-b-2-vinylpyridine) diblock copolymers (PS:P2PVP ratio 8200:8300, Polymer Source, Inc.) and toluene (ROTH, 99.5%) was prepared to form micellar cages. Then $FeCl_3$ (Sigma-Aldrich, 99.99%) was dissolved into the micellar solution and stirred for 48 h. The prepared micelles were deposited by dip coating onto Si(100) wafers having an oxide layer about 285 nm in thickness (provided by Sigert Wafer GmbH) and on an α-Al_2O_3(0001) single crystal substrate (SurfaceNet). The polymeric ligand was removed by exposure to O_2 plasma for 20 min (SPI Plasma Prep III Plasma Etcher operated at 20 W in 0.3 mbar of O_2). Then the samples were transferred into an UHV chamber through air.

In another set of experiments, Fe was deposited by PVD onto the same substrates from a Fe rod (99.99%, Goodfellow) using an e-beam assisted evaporator (Focus EFM4). Prior to the Fe deposition, the SiO_2/Si(100) and Al_2O_3(0001) substrates were annealed in UHV at 500 °C for 20 min and inspected by XPS.

XPS measurements were carried out in an UHV system (base pressure ~2 × 10^{-10} mbar) manufactured by SPECS. The spectra were collected using a monochromatic Al K_α X-ray source ($h\nu$ = 1486.6 eV) and a hemispherical analyzer (Phoibos 150). For energy calibration, we set the Si $2p_{3/2}$ level in SiO_2 at 103.3 eV and the Al $2p_{3/2}$ level in Al_2O_3 at 74.4 eV. Due to severe sample charging on the alumina single crystal in UHV, a flood gun (SPECS FG 15/40) was used for charge compensation. Spectra were processed using the CasaXPS software.

To study the structural transformations at catalytically relevant conditions, the "as prepared" samples were transferred into a high-pressure cell (SPECS HPC20) attached to the main UHV chamber through a gate valve. The sample was heated at a rate of 10 °C/min by the focused light of a halogen lamp through a quartz window. After treatment, the reactor was pumped out, and the sample was transferred back into the XPS chamber without exposure to air.

Powder catalysts were prepared by incipient wetness impregnation of γ-Al_2O_3 (Inframat, 99.99%) and SiO_2 (Strem Chemicals, 99%) powders with the Fe-containing micellar solution corresponding to an Fe loading of about 10 wt %. The catalysts were calcined in 1 atm of O_2 + Ar (1:1) at 400 °C for 6 h. The calcined catalysts were characterized by scanning transmission electron microscopy (STEM, FEI Talos F200X). The specific surface area of the powder catalysts was measured with Autosorb-1-C (Quantachrome Instrum.) using N_2 adsorption.

CO_2 hydrogenation reactions on the powdered catalysts were carried out in a fixed-bed mass flow reactor made of stainless steel, with the inside of the reactor tube coated by a glass liner. The samples were first reduced in pure H_2 (15 mL min^{-1}) for 2 h at 400 °C then cooled down to 300 °C, and subsequently the CO_2 + H_2 (1:3) reaction mixture was introduced into the reactor at 10 bar. The gas hourly space velocity (GHSV) was set to 3600 mL min^{-1} g^{-1} in all catalytic tests. The reaction was monitored using online gas chromatography coupled with mass spectrometry (GC/MS, Clarus 690GC-SQ8MS from PerkinElmer). The corresponding

mass spectra of each GC peak were analyzed using the NIST Mass Search Program (version 2.3).

XAS measurements at the Fe K-edge (7112.0 eV) were carried out at beamline BL 2-2 at Stanford Synchrotron Radiation Lightsource (SSRL). A Si(220) monochromator detuned by 45% was used for energy selection, and XAS data were collected in transmission mode. Ionization chambers, filled with pure N_2, were used to measure the intensity of the X-rays before and after the sample. The catalyst was diluted with silica in the 1:1 ratio and packed into a quartz capillary (1.0 mm diameter, wall thickness 10 μm) mounted into a Clausen cell.[29] Spectra alignment and normalization were performed using the Athena software.[30] Linear combination fitting of the XANES spectra was performed in the energy range between 7100 and 7230 eV, using spectra for an Fe foil, FeO and FeOOH as references for Fe(0), Fe(II) and Fe(III) states, respectively, and requiring the total concentration of Fe(0), Fe(II) and Fe(III) species to be equal to 100%. Extended X-ray absorption fine structure (EXAFS) data fitting was performed with the FEFFIT code,[30] using phase and amplitude functions obtained from *ab initio* calculations performed with the FEFF8.5 code for reference materials (bcc-Fe and FeO) to model contributions of Fe—Fe and Fe—O bonds, respectively. Fitting of $\chi(k)k^2$ spectra was carried out in *R*-space in the range from 0.6 to 3.0 Å. Fourier transforms were carried out in the *k* range from 2.0 to 9 Å^{-1}. To model the EXAFS spectra of the "as-prepared" samples, we only included the contribution of the Fe—O bond. Furthermore, the coordination number *N*, bond-length *R*, disorder factor σ^2, third cumulant of the bond-length distribution $c^{(3)}$, skewness of the distribution, and the correction to the photoelectron reference energy ΔE_0 were treated as fitting parameters. For the "reduced" samples, we additionally included two Fe—Fe paths corresponding to the first two coordination shells in bcc-Fe. To reduce the number of fitting variables for the reduced samples, we have set $c^{(3)}$ to 0 for all paths and σ^2 to be the same for both Fe—Fe paths and also assume that the ratios of the interatomic distances and coordination numbers for these paths are the same as for the ideal bcc-Fe structure. The amplitude reduction factor due to many-electronic processes (S_0^2 factor) was 0.74 ± 0.05 obtained from the fitting of the EXAFS spectrum for the Fe foil.

3. RESULTS AND DISCUSSION

Parts a and b of Figure 1 display typical AFM images of the micelle-synthesized Fe NPs deposited onto $SiO_2/Si(100)$ and $Al_2O_3(0001)$ substrates, respectively, obtained after dip-coating, and an oxygen plasma treatment was needed to remove the polymeric ligands. Since the lateral size of the particles imaged by AFM is overestimated due to the tip-NP convolution effect, the particle size is determined by analysis of their heights, which are 4.0 ± 1.1 nm and 4.4 ± 1.3 nm for NPs on SiO_2 and Al_2O_3 supports, respectively (see Figure S1 in the Supporting Information). The differences in the particle density can be attributed to different wetting behavior of the two oxide supports.

The chemical composition of the micellar NPs in different ambient conditions was investigated by NAP-XPS (Figure 2a,b). The Fe 2p spectra of the "as deposited" samples measured at room temperature in UHV are also shown for comparison. The binding energy (BE) of the Fe 2p$_{3/2}$ core level (thereafter only used in the discussion) at 711.4 eV (for Fe/SiO$_2$) and 711.0 eV (for Fe/Al$_2$O$_3$) and a weak satellite
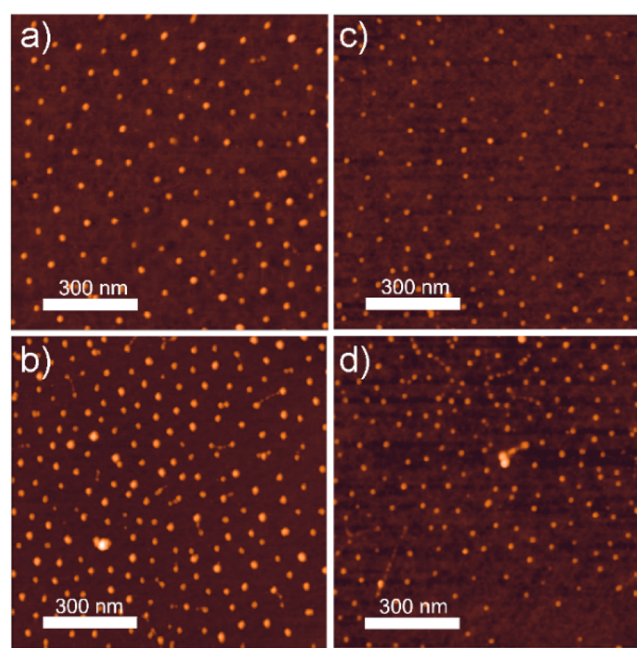

Figure 1. Typical AFM images of micellar Fe NPs deposited on (a) SiO$_2$/Si(001) and (b) Al$_2$O$_3$(0001) acquired after ligand removal. The same samples after the CO$_2$ hydrogenation NAP-XPS measurements are shown in (c) and (d), respectively.

("shake up") signal at around 719 eV are characteristic for Fe(III) species, as in hematite Fe$_2$O$_3$.[31−33] These species are formed during Fe NP synthesis and subsequent O$_2$-plasma treatment. Besides the Fe-related signals and those from the bare oxide support, XPS spectra revealed adventitious carbon (Figures S2 and S3) from the sample transfer into UHV through the air, which was removed by oxidation in 1 mbar of O$_2$ at 400 °C. The latter mimics the calcination procedure commonly used for the preparation of powder catalysts. The oxidation only slightly alters the Fe 2p lines, indicating that Fe in the "as prepared" samples is predominantly in the highest oxidation state 3+.

In the next step, the samples were exposed to 1 mbar of H$_2$ at 400 °C. This treatment is usually considered as an "activation" step for CO$_2$ hydrogenation catalysts.[2] On the Fe/SiO$_2$ sample, the Fe 2p$_{3/2}$ peak shifts by 1.6 eV toward lower BE (709.8 eV) and a weak satellite signal appears at ∼715 eV, thus indicating the formation of Fe(II) species, as in FeO. In addition, a new state appears as a shoulder at ∼706.6 eV (Figure 2a), which is characteristic of the metallic Fe(0) state. Therefore, Fe NPs on SiO$_2$ undergo reduction of Fe(III) to Fe(II) and partially to Fe(0), in general agreement with the reduction behavior of iron oxides (see, for instance, refs 34 and 35), commonly described as an Fe$_2$O$_3$ → Fe$_3$O$_4$ → FeO sequential transformation at these moderate temperatures. According to temperature-programmed reduction data,[34] the full reduction to Fe(0) only occurs at temperatures as high as 650 °C, although the complete reduction of Fe$_2$O$_3$ up to metallic Fe was reported after exposure to 0.2 mbar H$_2$ at 450 °C.[36]

When the sample is exposed to the CO$_2$ + H$_2$ reaction mixture (1:3, 1 mbar in total) at 300 °C, the intensity of the Fe(0) signal decreases, suggesting relative instability of the metallic state under reaction conditions. Since XPS spectra of metallic Fe and Fe carbides are similar and thus difficult to differentiate,[37,38] we also inspected the C 1s region (Figure
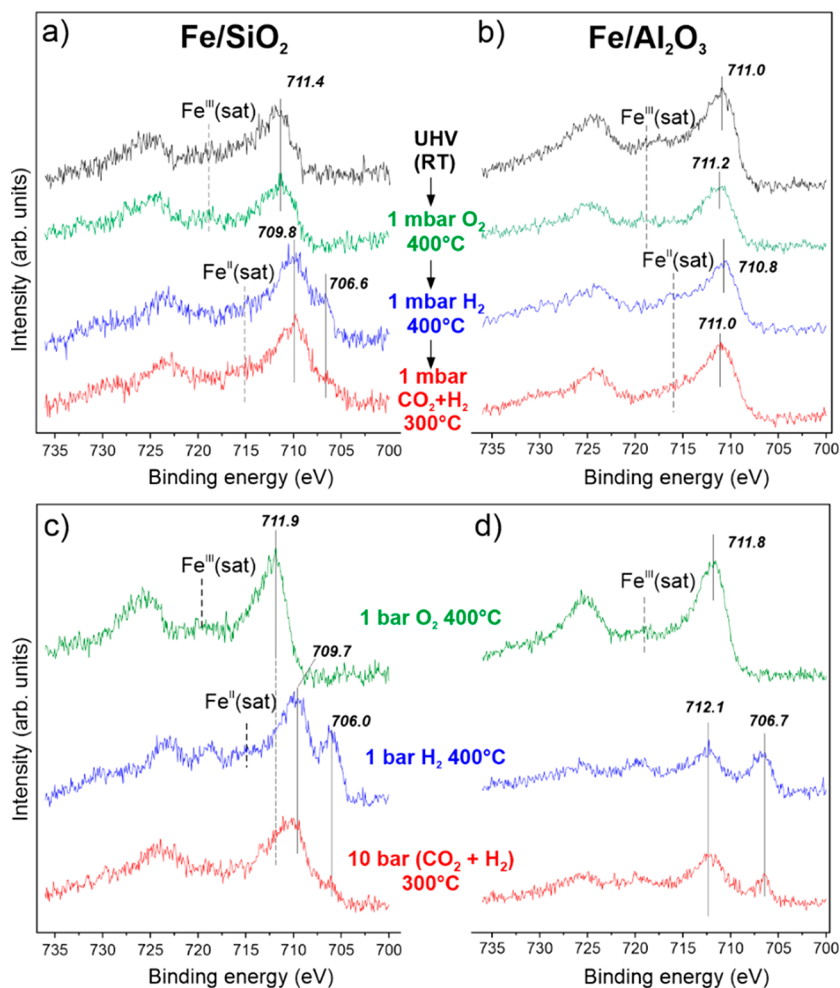
Figure 2. Fe 2p NAP-XPS spectra of micellar Fe NPs deposited onto (a,c) $SiO_2/Si(001)$ and (b,d) $Al_2O_3(0001)$ substrates. The measurement conditions are indicated adjacent to the spectra. (c,d) XPS spectra measured in UHV at room temperature after sample treatments as indicated.

S2), which only revealed traces of carbon at BEs around 284 eV, distinctly different from "carbidic" carbon BEs at 283 eV and below.[37] We therefore conclude that the Fe(0) phase, formed during activation in pure hydrogen, becomes oxidized in CO_2 hydrogenation reaction conditions.

The same type of experiments performed on the alumina-supported NPs revealed a different behavior (Figure 2b). When exposed to 1 mbar of H_2 at 400 °C, the main peak shifts to a lower BE by ∼0.4 eV only, substantially smaller than the 1.6 eV observed for Fe/SiO_2. Although the shift points to the partial reduction, Fe(III) species still dominate the surface. In addition, no metallic state is observed, that is again at variance with Fe/SiO_2. The Fe 2p spectrum remains virtually the same in the $CO_2 + H_2$ mixture at 300 °C. The lack of intensity at 706−707 eV provides clear evidence for the absence of both, metallic and iron carbide phases on the Fe/Al_2O_3 surface under CO_2 hydrogenation reaction conditions.

In summary, during the activation step the alumina support stabilizes Fe oxide in oxidation state 3+, whereas NPs supported on silica can be readily reduced in pure hydrogen to Fe(II) and partially to the metallic Fe(0) state. However, both catalysts showed neither metallic nor carbide phase under the CO_2 hydrogenation reaction conditions. Post characterization of the samples by AFM (Figure 1c,d) revealed neither particle sintering nor aggregation on both model catalysts.

In order to address whether the results from the NAP-XPS experiments are the result of kinetic limitations, due to being performed at lower pressure to catalytically relevant pressure, we performed XPS measurements on the samples exposed sequentially to 1 bar O_2 at 400 °C, then 1 bar H_2 at 400 °C, and finally, to 10 bar of the $CO_2 + H_2$ (1:3) reaction mixture at 300 °C using a high-pressure cell. After each treatment, the cell was evacuated, and the sample cooled and transferred into the analysis chamber through vacuum (i.e., without exposure to air). XPS spectra were recorded in UHV at room temperature. The Fe 2p region is displayed in Figures 2c,d, while the corresponding Si 2p, Al 2p, O 1s, and C 1s spectra are shown in Figures S4 and S5.

Following the oxidation step, the Fe 2p spectra for both supports are similar and only revealed Fe(III) species. Note, however, that the Fe $2p_{3/2}$ BEs observed at 1 bar (711.9 and 711.8 eV, for silica and alumina supports, respectively) are higher than those for the samples oxidized at 1 mbar (711.4 and 711.2 eV, respectively).

After the pure hydrogen treatment the Fe(0) component in the SiO_2-supported NPs increases considerably at 1 bar and shifts to lower BE, i.e., from 706.6 to 706.0 eV, while the Fe(II) peak stays at 709.7 (±0.1) eV (Figure 2c). However, the Fe(0) signal disappears after the CO_2 hydrogenation reaction at 10 bar, and the spectrum becomes similar to that measured in the reaction mixture at 1 mbar at 300 °C.
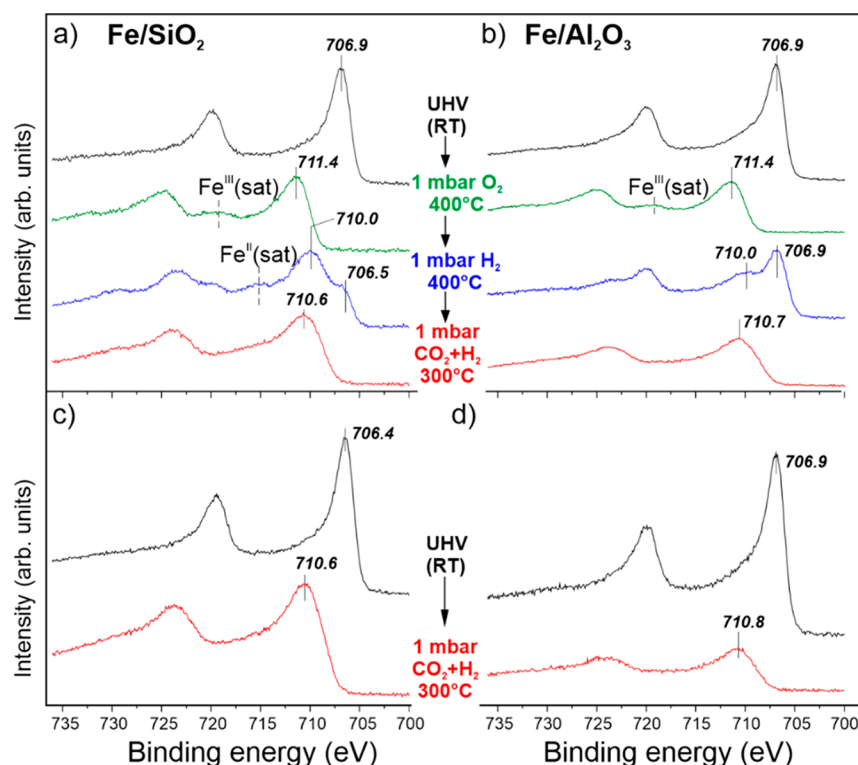
Figure 3. Fe 2p NAP-XPS spectra obtained on PVD-deposited Fe NPs on $SiO_2/Si(001)$ (a,c) and $Al_2O_3(0001)$ (b,d) substrates at the conditions indicated adjacent to the spectra. In panels (c,d), the samples were exposed directly to the reaction atmosphere omitting oxidation and reduction treatments.

A more pronounced H_2 pressure effect is observed for the Al_2O_3-supported NPs (Figure 2d): a strong Fe(0) signal shows up at 706.7 eV at 1 bar, which was not present in the NAP-XPS spectra at 1 mbar. The Fe(III) peak decreases and slightly shifts to higher BE (from 711.8 to 712.1 eV). Note also that the integral intensity of the Fe 2p signal is considerably reduced, in contrast to the silica-supported NPs. The loss of intensity can be indicative either of the NP shape change and/ or partial Fe migration into the alumina support. Nonetheless, after the CO_2 hydrogenation reaction, the signal at 706.7 eV decreases, whereas the Fe(III) signal gains in intensity. Since the inspection of the C 1s region revealed no carbon on this sample (Figure S5), we can safely assign the 706.7 eV signal to the metallic Fe surface and not to iron carbide.

Thus, we conclude that the oxide support does play a role in the chemical transformations of the iron oxide NPs. Alumina stabilizes the Fe(III) oxide even in the hydrogen atmosphere, while silica is rather "passive" with respect to the Fe(III) reduction to Fe(II), which readily occurs on unsupported iron oxides.

The results presented above were obtained on supported NPs prepared by an inverse micelle encapsulation method, which needed exposure to oxygen plasma for ligand removal, thus leading to oxidation of the as-prepared Fe NPs. To examine whether the iron precursor or the sample preparation method alter the chemistry of the supported NPs in the CO_2 hydrogenation reaction, we investigated another planar model system, where Fe NPs were prepared by PVD of Fe onto the same substrates. Note, however, that the PVD preparation results in a much higher NP density on the support surface as compared to that of the samples synthesized from the micellar

precursor (see also refs 37 and 39). The typical morphology of the PVD samples observed by AFM is shown in Figure S6.

Figure 3 summarizes NAP-XPS results for the Fe 2p region in the PVD-prepared samples (other core levels of interest are presented in Figures S7 and S8). The spectra for "as deposited" Fe NPs on both supports, measured in UHV at room temperature, showed the Fe $2p_{3/2}$ peak at 706.9 eV (Figure 3a,b), henceforth used as the internal reference for the metallic Fe(0) state, although the value may slightly deviate depending on the particle size due to the so-called "final state" effects.[40] Upon exposure to 1 mbar of O_2, the particles become fully oxidized giving rise to the Fe $2p_{3/2}$ peak at 711.4 eV and the "shake up" satellite at ~719 eV, both characteristic of Fe(III). In fact, the oxidation occurs even at room temperature (not shown here), in full agreement with refs 41 and 42.

Upon subsequent exposure to a hydrogen atmosphere (Figure 3a), the Fe 2p spectrum for the Fe/SiO_2 sample shifts to lower BEs by 1.4 eV (710.0 eV), and a weak satellite signal appears at ~715 eV, both indicating the formation of the Fe(II) oxide. In addition, a new state shows up at 706.5 eV, suggesting the partial reduction to Fe(0). A similar behavior is also observed for Fe/Al_2O_3 (Figure 3b), although the relative intensity of the Fe(0) signal at 706.9 eV is substantially higher than for Fe/SiO_2. For both catalysts, the Fe(0) state disappears in the $CO_2 + H_2$ mixture. The spectra shift to higher BEs (710.6 ± 0.1 eV), and the Fe(II) satellite signal at ~715 eV attenuates, all indicating the partial oxidation of Fe(II) to Fe(III) in the presence of CO_2. Therefore, CO_2 acts as an oxidizing agent for metallic Fe even in excess of H_2 in the reaction atmosphere. Actually, the blank experiments using pure CO_2 showed that CO_2 readily oxidizes metallic Fe at room temperature (see also ref 43). Once oxidized, the surface
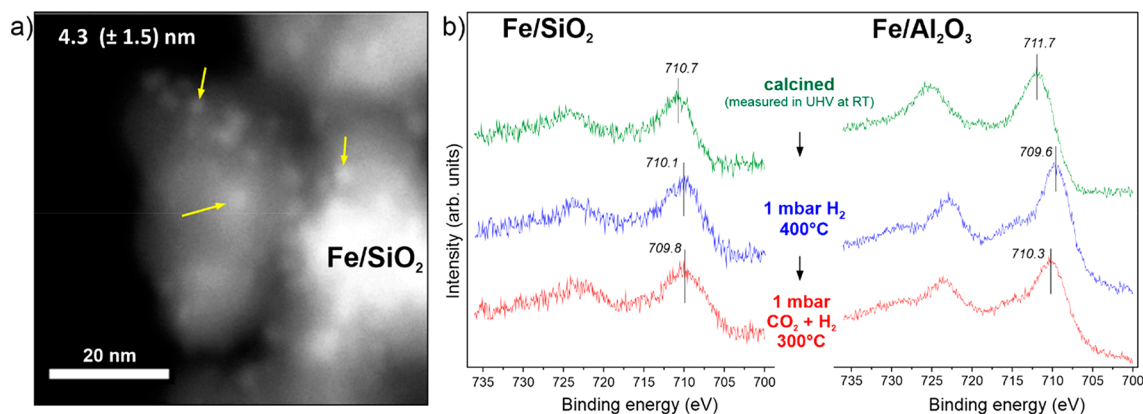
Figure 4. (a) STEM-HAADF image of the Fe/SiO$_2$ catalysts prepared by impregnation with the Fe micellar precursor and subsequent calcination in oxygen. The arrows mark some Fe NPs for clarity. (b) NAP-XPS spectra measured on the powder catalysts at the conditions indicated.

cannot be reduced to the metallic state by hydrogen in the reaction mixture at 300 °C as it cannot be reduced even in pure H$_2$ at 400 °C (see Figure 3a,b). In addition, the water produced via the r-WGS reaction pathway in the CO$_2$ + H$_2$ mixture is also expected to facilitate the oxidation of Fe.

The chemical state of Fe under the CO$_2$ hydrogenation conditions is rather independent of the sample prehistory. Direct exposure of the pure metallic NPs to the reaction atmosphere (Figure 3c,d) results in the same spectra as for the samples subjected to oxidation−reduction treatments prior to the reaction (Figure 3a,b). No "pre-history" effect is expected for the micellar samples as well, since the Fe-oxide phase dominates both the "as prepared" and "oxidized-reduced" NPs. Again, the formation of Fe carbide is not observed under reaction conditions, in full agreement with the NAP-XPS results obtained on the samples prepared using the micellar precursor.

Comparison of the Fe 2p NAP-XPS spectra obtained for the Fe/SiO$_2$ model catalysts prepared using two methods (see Figures 2a and 3a) revealed no difference in O$_2$ and H$_2$ atmospheres, and only a deviation (∼0.7 eV) in the peak position when exposed to CO$_2$ + H$_2$, reflecting different Fe(II):Fe(III) ratios in the latter sample. For Fe/Al$_2$O$_3$, the most striking difference between the two preparation methods is the degree of reduction observed in pure hydrogen ambient, which is substantial for the PVD-prepared system and close to zero for the micellar samples. (In principle, this finding may be indicative of different NP/Al$_2$O$_3$ interfaces formed upon deposition of metallic Fe by PVD, in the former case, and of polymer-covered Fe-oxide NPs, in the latter.) Nevertheless, the spectra recorded on these two Fe/Al$_2$O$_3$ samples in the CO$_2$ hydrogenation atmosphere are very similar (710.6 vs 711.0 eV) and do not show Fe(0) species.

Therefore, all our NAP-XPS results, obtained on different oxide supported model catalysts, demonstrate that, independently of the initial state of the iron NPs before the CO$_2$ hydrogenation reaction, the NPs' surface under the reaction conditions contains a mixture of Fe(II) and Fe(III) species, with no indication of the carbide phase.

To link the results obtained on planar model systems to supported powder catalysts, we prepared catalysts by impregnation of high surface area silica and alumina powders with the same Fe colloidal precursor. The specific surface areas of the calcined catalysts (157 and 129 m^2 g^{-1} for Fe/Al$_2$O$_3$ and Fe/SiO$_2$, respectively) and adsorption isotherms (see Figure

S9) reflect the nonporous, but nanoparticulate structure of the oxide supports used. The average particle size (4.3 ± 1.5 nm) of the Fe NPs supported on SiO$_2$ determined by STEM (Figure 4a, Figure S10) is very close to that of observed by AFM on the planar samples (Figure 1).

The electronic state of iron in the powder catalysts was inspected by NAP-XPS on the samples prepared by drop casting onto a flat silica substrate. Figure 4b displays the Fe 2p spectra, which are, in fact, similar to the spectra obtained on the planar systems (Figure 2a,b). No metallic Fe is detected in pure hydrogen at 400 °C as well as in the CO$_2$ + H$_2$ reaction atmosphere at 300 °C. All spectral changes can be explained in terms of the different Fe(II):Fe(III) ratios at the NP surface.

The nanocrystalline powder catalysts were tested in the CO$_2$ hydrogenation reaction under conditions typical for this reaction.[4] The main results are summarized in Figure 5 and
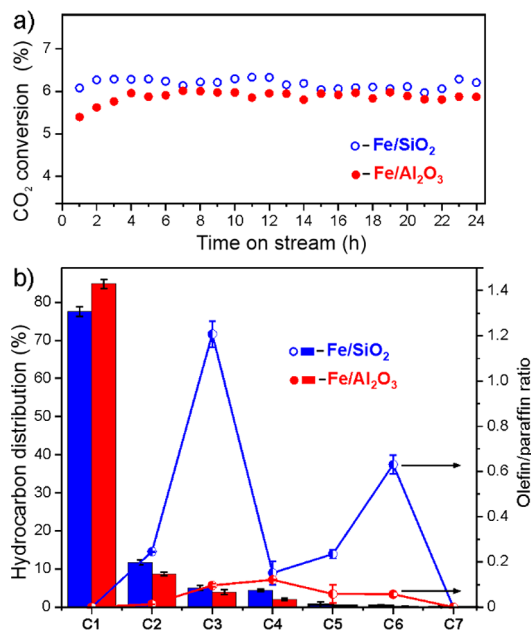

Figure 5. Catalytic tests of 10 wt % Fe NPs impregnated on nanocrystalline SiO$_2$ and Al$_2$O$_3$ powder supports in the CO$_2$ hydrogenation reaction (300 °C, 10 bar of H$_2$ + CO$_2$ (3:1), GHSV = 3600 mL min^{-1} g^{-1}). (a) CO$_2$ conversion as a function of the reaction time and (b) product selectivity showing the hydrocarbon distribution (left axis) and olefin/paraffin ratio (right axis).

Table 1. Basically, the catalytic characteristics (conversion and selectivity) fall in the range reported in the literature for Fe/

Table 1. Catalytic Testing of the Fe/SiO₂ and Fe/Al₂O₃ Nanocrystalline Powder Catalysts in Steady State[a]

catalysts	CO_2 conversion (%)	selectivity (%)			total olefin/paraffin ratio
		CO	CH₄	C₂₊	
Fe/SiO₂	6.2	70	23	7	0.36
Fe/Al₂O₃	5.9	61	33	6	0.05

[a]Reaction conditions: 300 °C, 10 bar, H_2: CO_2 = 3:1 ratio, GHSV = 3600 mL min⁻¹ g⁻¹.

Al_2O_3[44] and Fe/ZrO_2[20] catalysts prepared by the incipient wetness impregnation. Our catalysts primarily produce CO and CH₄, with Fe/Al₂O₃ showing higher activity for methane as compared to Fe/SiO₂. However, a major difference in the product distribution is the olefin/paraffin ratio, which is substantially higher on the silica-supported catalyst, showing rather a complex pattern of the hydrocarbon products (Figure 5b, see also Figures S11–13).

The catalysts were further investigated by XAS *in situ*. In particular, the X-ray absorption near edge structure (XANES) allows quantitative determination of the Fe oxidation state *in situ*.[11,16,45,46] XANES spectra of the "as prepared" and subsequently calcined samples (Figure 6c) match well those of goethite FeOOH and hematite Fe_2O_3 with iron in the 3+ state, *i.e.*, in full agreement with the XPS results (Figure 2). Considerable changes are observed upon heating to 400°C in the H_2/He (1:4) atmosphere, with the spectral evolution proceeding differently for the two catalysts (Figure 6a,b). In particular, the shoulder at ~7115 eV at the onset of the FeK-edge, which develops with time and closely resembles that in the metallic Fe foil, is more intense in the Fe/SiO₂ than Fe/

Al_2O_3 sample. Linear combination fitting analysis of the XANES spectra using an Fe foil, FeO and FeOOH compounds as references (see the representative fits in Figure S14) revealed that the "as-prepared" catalysts contain mostly Fe(III) species, with a small contribution of Fe(0) (Figure 7). During heating in H_2/He, both samples become partially reduced, and Fe(III) species transformed into Fe(II) and Fe(0). However, the fraction of metallic iron in Fe/Al₂O₃ is significantly lower than in Fe/SiO₂ (65 and 85% (±4%), respectively), indicating that Fe-oxide NPs on the alumina support are more resistant toward reduction in hydrogen, in agreement with the NAP-XPS results (Figure 2).

EXAFS spectra of the Fe K-edge are displayed in Figure 8b. The main characteristics of the Fe coordination sphere derived from the EXAFS spectra are summarized in Table 2 (all fitting parameters are presented in Table S1). EXAFS data for the "as prepared" samples showed Fe(III) species like in FeOOH (Figure 8a), in full agreement with the XANES results. The slightly reduced Fe–O coordination numbers as compared to the reference can be attributed to a disordered, defective structure of our NPs. After the reduction treatment, the Fe–O related scattering path attenuates, and the main peak in the Fourier-transformed (FT) EXAFS (Figure 8b) shifts from 1.6 to 2.4 Å (phase uncorrected), indicating the formation of the Fe–Fe bonds. Data fitting procedure (Figure 8b and Table 2) confirmed that the main peak in the FT-EXAFS of the reduced samples is dominated by the two nearest Fe–Fe coordination shells in bcc-like Fe, in addition to Fe–O bonds, suggesting that Fe reduction is not complete, in agreement with the above-presented XANES results.

The Fe–O coordination numbers are higher, and concomitantly the Fe–Fe coordination numbers are lower in the reduced Fe/Al₂O₃ sample as compared to reduced Fe/SiO₂, which is in agreement with the higher contribution of oxidized species remained in the alumina supported catalysts upon
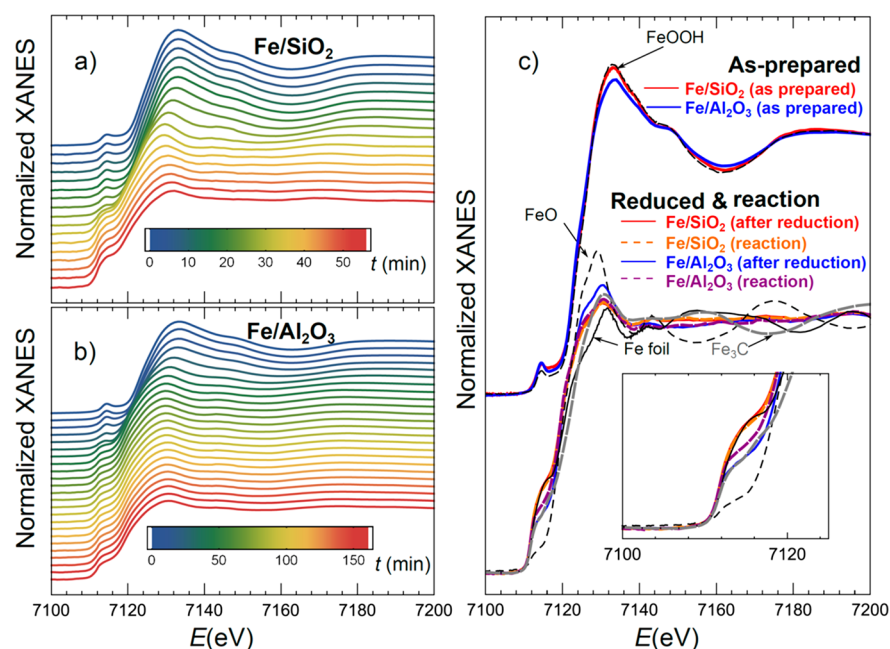

Figure 6. Fe K-edge XANES spectra measured on micellar Fe NPs supported on (a) SiO₂ and (b) Al₂O₃ powders during heating (10 °C/min) from room temperature to 400 °C in a H_2/He (1:4) mixture at 1 bar. The spectra are offset for clarity. (c) Comparison of the spectra in the "as-prepared" samples, after reduction in H_2 and cooling to room temperature, and under reaction conditions in 10 bar of CO_2 + H_2 (1:3) at 300 °C. Spectra for reference compounds (Fe foil, FeO, Fe₃C, and FeOOH) are shown for comparison.
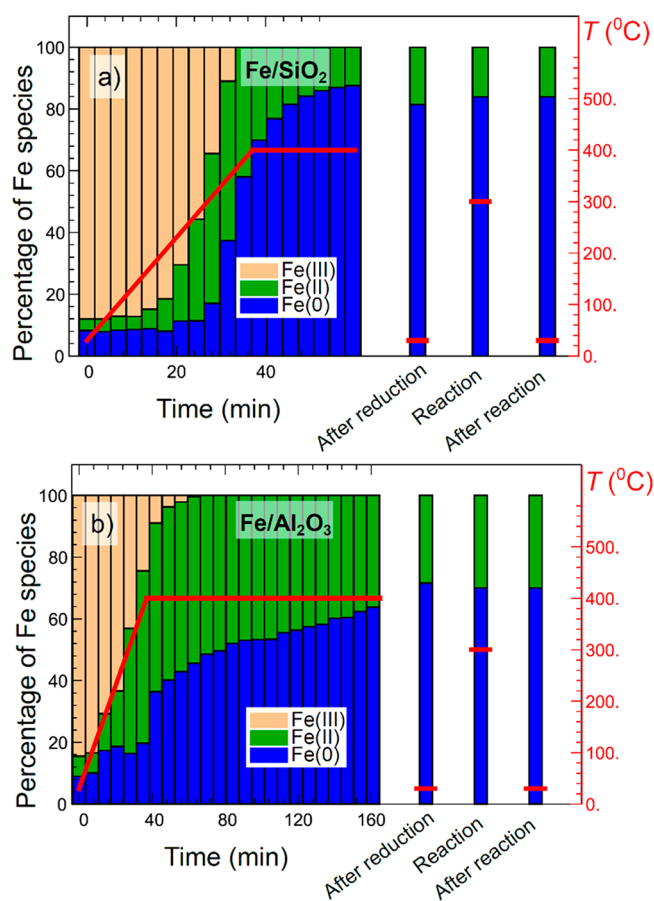
Figure 7. Relative concentration of different iron species in Fe/SiO$_2$ (a) and Fe/Al$_2$O$_3$ (b) catalysts determined by linear combination analysis of the spectra shown in Figure 4a,b. The red line shows the temperature profile and referenced to the y-axis on the right. The three separate columns show the results for the sample reduced in H$_2$ at 400 °C and cooled to room temperature, under reaction conditions at 300 °C, and after cooling the samples to room temperature. Red horizontal lines indicate the measurement temperature.

reduction, as observed by XANES. Interestingly, while Fe−Fe bond length obtained by EXAFS agree well with those in iron bulk, the Fe−O bond lengths (1.98−2.00 Å) is considerably shorter than in bulk FeO (∼2.2 Å) suggesting that the Fe(II) oxide phase in the reduced samples is different from the bulk-like FeO and probably disordered.

To monitor the state of the catalysts under reaction conditions, we performed XANES measurements in 10 bar of the CO$_2$ + H$_2$ (1:3) reaction mixture at 300 °C. In addition, both XANES and EXAFS spectra were measured after reducing the pressure to 1 bar and cooling the samples to room temperature (rt). XANES (Figure 6c and Figure 7) and EXAFS (Figure 8 and Table 2) data all showed no significant changes of the Fe oxidation state when compared to the reduced NPs. Note, however, the decrease in the Fe−Fe coordination numbers observed by EXAFS on the spent catalysts (1 bar, rt), which can be attributed to changes in the catalyst morphology.

Importantly, XANES spectra of the reduced samples and those in the reaction atmosphere differ significantly from that of a Fe$_3$C carbide reference. This is most clearly seen in the pre-edge region (zoomed in the inset in Figure 6c), where the signal intensity in the reduced catalysts is substantially higher

than that of the Fe$_3$C reference, allowing us to differentiate metallic and carbide phases.[11] Note also that the EXAFS oscillations in k-space (see Figure 8a) for the reduced samples match well those of the metallic Fe foil and are clearly different from iron carbide Fe$_3$C.

Therefore, an iron carbide phase was not observed under reaction conditions, thus fully supporting the XPS-based conclusion about the absence of Fe−carbide surface layers in the model catalysts. However, there is a difference between the XAS and the XPS results regarding the state of the catalyst in the CO$_2$ + H$_2$ mixture. While XAS revealed no significant changes if compared to the reduced catalysts as far as the oxidation state of Fe in the NPs is concerned, and the chemical composition of the catalyst is described as a mixture of Fe(II) and Fe(0) species, XPS data showed the reoxidation of the catalyst so that the Fe(0) signal disappears, and Fe(II) is partially oxidized to the Fe(III) state. Such a discrepancy cannot be explained solely by the different morphology of the oxide supports investigated by XAS and XPS (nanocrystalline powder vs planar substrates, respectively), since NAP-XPS spectra revealed very similar spectral evolution of the Fe 2p state in the micelles deposited on both flat and powder supports (cf. Figures 2a,b and 4b). However, XPS is more surface sensitive as compared to XAS that probes primarily the bulk phase of the NPs. Indeed, for the Al Kα X-ray source used, the escape depth of the Fe 2p photoelectrons in Fe and Fe oxides is about 1.2 and 1.6 nm, respectively. Therefore, the difference in the phase composition formed under reaction conditions determined by XAS and XPS most likely originate from different phases constituting the surface and the bulk of the NPs. Accordingly, the Fe NPs in CO$_2$ hydrogenation atmosphere expose an oxide-rich surface, while the particles' core is metal-rich.

Turning back to the CO$_2$ hydrogenation activity of our model catalysts (Figure 5), we notice that the difference observed in the olefin/paraffin ratio for the two catalysts correlates with a considerably higher concentration of Fe(II) species at the NP surface in the Fe/SiO$_2$ catalysts as compared to Fe/Al$_2$O$_3$ (both after reaction at 10 bar, see Figure 2c,d). It appears that Fe(II) leads to a larger amount of olefins in the hydrocarbon products, whereas Fe(III) to paraffins.

4. SUMMARY AND CONCLUSIONS

In this work, we studied the structure and composition of Fe-based catalysts, commonly employed for the hydrogenation of CO$_2$ toward high-order hydrocarbons. Specifically, we monitored the chemical evolution of oxide supported iron nanoparticles during calcination (oxidation) and reduction (activation) pretreatments as well as in the CO$_2$ hydrogenation reaction using NAP-XPS in the mbar range of pressures. The NAP-XPS results showed the formation of both, Fe(III) and Fe(II) oxides on the NP surface under CO$_2$ hydrogenation reaction conditions, independently of the iron precursor and the oxide support. It appears, however, that the alumina support stabilizes the higher oxidation state (3+) of iron. In contrast to previous studies performed on unsupported Fe catalysts, an iron carbide phase was never observed in our catalysts, even at catalytically relevant conditions, i.e., 10 bar of CO$_2$ + H$_2$ (1:3) at 300 °C. The latter experiments, conducted on powder samples prepared by impregnation of nanocrystalline SiO$_2$ and Al$_2$O$_3$ with Fe-containing micelles, revealed similar findings as those obtained by NAP-XPS. We associate the effects with the nanometer size of the Fe particles, which
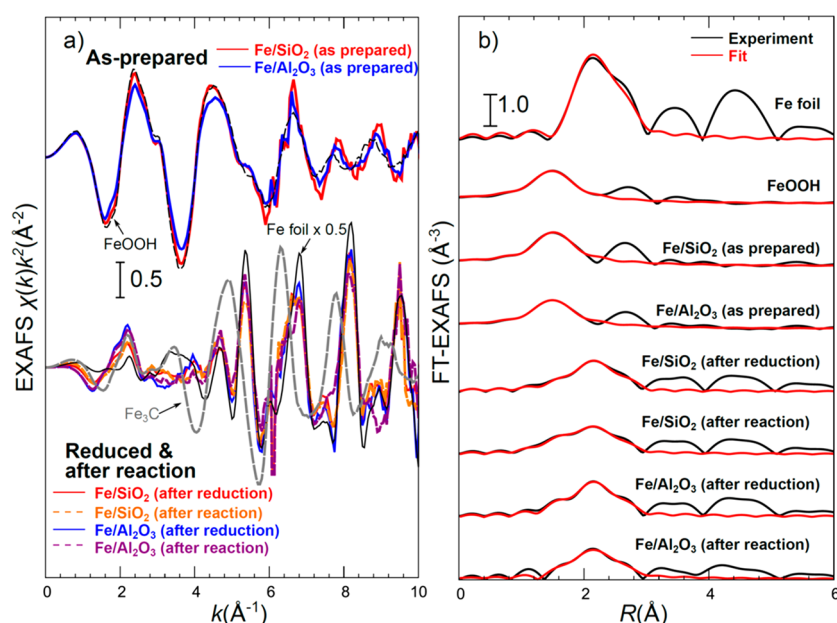
Figure 8. Fe K-edge EXAFS spectra (a) and their Fourier transforms (b) for micellar Fe NPs supported on SiO_2 and Al_2O_3 (as prepared, after reduction in hydrogen, and after reaction in $CO_2 + H_2$ (1:3)) all acquired in the corresponding gas atmosphere after cooling the samples to room temperature. The spectra are offset for clarity. Spectra for reference compounds (Fe foil, Fe_3C, and FeOOH) are shown for comparison. Results of EXAFS data fitting are shown in (b).

Table 2. Coordination Numbers N and Interatomic Distances R Obtained from the Fitting of Experimental Fe K-Edge EXAFS Data[a]

sample	N_{Fe-O}	R_{Fe-O} (Å)	N_{Fe-Fe}	R_{Fe-Fe} (Å)
Fe foil			8	2.47(1)
			6	2.86(1)
FeOOH	6.1(1)	2.004(8)		
Fe/SiO₂ (as prepared)	5.4(3)	2.02(2)		
Fe/SiO₂ (after reduction in H₂)	1.1(4)	1.98(1)	5.0(7)	2.47(1)
			3.8(5)	2.86(1)
Fe/SiO₂ (after CO₂ + H₂ reaction)	1.1(1)	1.94(1)	2.9(5)	2.47(1)
			2.2(3)	2.85(1)
Fe/Al₂O₃ (as prepared)	4.9(1)	2.01(1)		
Fe/Al₂O₃ (after reduction in H₂)	1.5(1)	2.00(1)	4.0(2)	2.47(1)
			3.0(2)	2.85(1)
Fe/Al₂O₃ (after CO₂ + H₂ reaction)	0.7(4)	2.02(2)	3.4(2)	2.48(2)
			2.5(1)	2.87(2)

[a]The error bar is given in parentheses.

undergo strong interaction with the oxide support. The combined XPS (which are more surface sensitive) and XAS results (probing both the surface and the bulk) favor the model of Fe NP consisting of a metal-rich core and oxide-rich shell under the CO_2 hydrogenation reaction conditions.

The catalytic tests provide solid evidence for hydrocarbon production on the Fe oxide surface, which is considered active primarily for the r-WGS reaction producing CO. Interestingly, the olefin/paraffin product ratio was found to be dependent on the nature of the support, which influences the final oxidation state of the Fe NPs during the reaction as well as their structure. Since many recent FTS and CO_2–FTS studies point to iron carbide as the key phase for the production of high-order hydrocarbons (C_{5+}), the iron oxide catalysts presented here remain promising for light hydrocarbon production. In this respect, "surface-science" oriented studies in combination

with *operando* XAS measurements provide a playground for the rational design of Fe-based catalysts selective for high value-added light olefins.

ASSOCIATED CONTENT

Supporting Information

The Supporting Information is available free of charge at https://pubs.acs.org/doi/10.1021/acscatal.1c01549.

> Particle size distribution; XPS spectra of Si 2p, Al 2p, O 1s and C 1s regions; N_2 adsorption isotherms; TEM images of Fe/SiO₂; GC/MS results of reaction products; fitting and structure parameters for Fe K-edge XANES and EXAFS spectra (PDF)

AUTHOR INFORMATION

Corresponding Author

Shamil Shaikhutdinov − *Department of Interface Science, Fritz Haber Institute of the Max Planck Society, 14195 Berlin, Germany;* orcid.org/0000-0001-9612-9949; Email: shaikhutdinov@fhi-berlin.mpg.de

Authors

Mauricio Lopez Luna − *Department of Interface Science, Fritz Haber Institute of the Max Planck Society, 14195 Berlin, Germany*

Janis Timoshenko − *Department of Interface Science, Fritz Haber Institute of the Max Planck Society, 14195 Berlin, Germany*

David Kordus − *Department of Interface Science, Fritz Haber Institute of the Max Planck Society, 14195 Berlin, Germany*

Clara Rettenmaier − *Department of Interface Science, Fritz Haber Institute of the Max Planck Society, 14195 Berlin, Germany*

See Wee Chee − *Department of Interface Science, Fritz Haber Institute of the Max Planck Society, 14195 Berlin, Germany*

Adam S. Hoffman − *SSRL, SLAC National Accelerator Laboratory, Menlo Park, California 94025, United States*

Simon R. Bare − *SSRL, SLAC National Accelerator Laboratory, Menlo Park, California 94025, United States*

Beatriz Roldan Cuenya − *Department of Interface Science, Fritz Haber Institute of the Max Planck Society, 14195 Berlin, Germany;* ⦿ orcid.org/0000-0002-8025-307X

Notes

The authors declare no competing financial interest.

■ REFERENCES

(1) Porosoff, M. D.; Yan, B.; Chen, J. G. Catalytic reduction of CO_2 by H2 for synthesis of CO, methanol and hydrocarbons: challenges and opportunities. *Energy Environ. Sci.* **2016**, *9* (1), 62−73.

(2) Li, W.; Wang, H.; Jiang, X.; Zhu, J.; Liu, Z.; Guo, X.; Song, C. A short review of recent advances in CO_2 hydrogenation to hydrocarbons over heterogeneous catalysts. *RSC Adv.* **2018**, *8* (14), 7651−7669.

(3) Gnanamani, M. K.; Jacobs, G.; Hamdeh, H. H.; Shafer, W. D.; Liu, F.; Hopps, S. D.; Thomas, G. A.; Davis, B. H. Hydrogenation of Carbon Dioxide over Co−Fe Bimetallic Catalysts. *ACS Catal.* **2016**, *6* (2), 913−927.

(4) Choi, Y. H.; Jang, Y. J.; Park, H.; Kim, W. Y.; Lee, Y. H.; Choi, S. H.; Lee, J. S. Carbon dioxide Fischer−Tropsch synthesis: A new path to carbon-neutral fuels. *Appl. Catal., B* **2017**, *202*, 605−610.

(5) Wei, J.; Sun, J.; Wen, Z.; Fang, C.; Ge, Q.; Xu, H. New insights into the effect of sodium on Fe_3O_4- based nanocatalysts for CO_2 hydrogenation to light olefins. *Catal. Sci. Technol.* **2016**, *6* (13), 4786−4793.

(6) Kishan, G.; Lee, M.-W.; Nam, S.-S.; Choi, M.-J.; Lee, K.-W. The catalytic conversion of CO_2 to hydrocarbons over Fe−K supported on Al_2O_3−MgO mixed oxides. *Catal. Lett.* **1998**, *56* (4), 215−219.

(7) Amoyal, M.; Vidruk-Nehemya, R.; Landau, M. V.; Herskowitz, M. Effect of potassium on the active phases of Fe catalysts for carbon dioxide conversion to liquid fuels through hydrogenation. *J. Catal.* **2017**, *348*, 29−39.

(8) Shroff, M. D.; Kalakkad, D. S.; Coulter, K. E.; Kohler, S. D.; Harrington, M. S.; Jackson, N. B.; Sault, A. G.; Datye, A. K. Activation of Precipitated Iron Fischer−Tropsch Synthesis Catalysts. *J. Catal.* **1995**, *156* (2), 185−207.

(9) Li, S.; Ding, W.; Meitzner, G. D.; Iglesia, E. Spectroscopic and Transient Kinetic Studies of Site Requirements in Iron-Catalyzed Fischer−Tropsch Synthesis. *J. Phys. Chem. B* **2002**, *106* (1), 85−91.

(10) Chang, Q.; Zhang, C.; Liu, C.; Wei, Y.; Cheruvathur, A. V.; Dugulan, A. I.; Niemantsverdriet, J. W.; Liu, X.; He, Y.; Qing, M.; Zheng, L.; Yun, Y.; Yang, Y.; Li, Y. Relationship between Iron Carbide Phases (ε-Fe_2C, Fe_7C_3, and χ-Fe_5C_2) and Catalytic Performances of Fe/SiO_2 Fischer−Tropsch Catalysts. *ACS Catal.* **2018**, *8* (4), 3304−3316.

(11) de Smit, E.; Cinquini, F.; Beale, A. M.; Safonova, O. V.; van Beek, W.; Sautet, P.; Weckhuysen, B. M. Stability and Reactivity of ϵ−χ−θ Iron Carbide Catalyst Phases in Fischer−Tropsch Synthesis: Controlling μ_C. *J. Am. Chem. Soc.* **2010**, *132* (42), 14928−14941.

(12) Paalanen, P. P.; Weckhuysen, B. M. Carbon Pathways, Sodium-Sulphur Promotion and Identification of Iron Carbides in Iron-based Fischer−Tropsch Synthesis. *ChemCatChem* **2020**, *12* (17), 4202−4223.

(13) Puga, A. V. On the nature of active phases and sites in CO and CO_2 hydrogenation catalysts. *Catal. Sci. Technol.* **2018**, *8* (22), 5681−5707.

(14) Wei, J.; Ge, Q.; Yao, R.; Wen, Z.; Fang, C.; Guo, L.; Xu, H.; Sun, J. Directly converting CO_2 into a gasoline fuel. *Nat. Commun.* **2017**, *8* (1), 15174.

(15) Zhang, Y.; Fu, D.; Liu, X.; Zhang, Z.; Zhang, C.; Shi, B.; Xu, J.; Han, Y.-F. Operando Spectroscopic Study of Dynamic Structure of Iron Oxide Catalysts during CO_2 Hydrogenation. *ChemCatChem* **2018**, *10* (6), 1272−1276.

(16) Chew, L. M.; Kangvansura, P.; Ruland, H.; Schulte, H. J.; Somsen, C.; Xia, W.; Eggeler, G.; Worayingyong, A.; Muhler, M. Effect of nitrogen doping on the reducibility, activity and selectivity of carbon nanotube-supported iron catalysts applied in CO_2 hydrogenation. *Appl. Catal., A* **2014**, *482*, 163−170.

(17) Suo, H.; Wang, S.; Zhang, C.; Xu, J.; Wu, B.; Yang, Y.; Xiang, H.; Li, Y.-W. Chemical and structural effects of silica in iron-based Fischer−Tropsch synthesis catalysts. *J. Catal.* **2012**, *286*, 111−123.

(18) Ahmadi, M.; Mistry, H.; Roldan Cuenya, B. Tailoring the Catalytic Properties of Metal Nanoparticles via Support Interactions. *J. Phys. Chem. Lett.* **2016**, *7* (17), 3519−3533.

(19) Zhang, Y.; Qing, M.; Wang, H.; Liu, X.-W.; Liu, S.; Wan, H.; Li, L.; Gao, X.; Yang, Y.; Wen, X.-D.; Li, Y.-W. Comprehensive understanding of SiO_2-promoted Fe Fischer−Tropsch synthesis catalysts: Fe-SiO_2 interaction and beyond. *Catal. Today* **2020**, 96−105.

(20) Zhu, J.; Zhang, G.; Li, W.; Zhang, X.; Ding, F.; Song, C.; Guo, X. Deconvolution of the Particle Size Effect on CO_2 Hydrogenation over Iron-Based Catalysts. *ACS Catal.* **2020**, *10* (13), 7424−7433.

(21) Vogt, C.; Groeneveld, E.; Kamsma, G.; Nachtegaal, M.; Lu, L.; Kiely, C. J.; Berben, P. H.; Meirer, F.; Weckhuysen, B. M. Unravelling structure sensitivity in CO_2 hydrogenation over nickel. *Nature Catalysis* **2018**, *1* (2), 127−134.

(22) Arble, C.; Jia, M.; Newberg, J. T. Lab-based ambient pressure X-ray photoelectron spectroscopy from past to present. *Surf. Sci. Rep.* **2018**, *73* (2), 37−57.

(23) Salmeron, M.; Schlögl, R. Ambient pressure photoelectron spectroscopy: A new tool for surface science and nanotechnology. *Surf. Sci. Rep.* **2008**, *63* (4), 169−199.

(24) Lundgren, E.; Zhang, C.; Merte, L. R.; Shipilin, M.; Blomberg, S.; Hejral, U.; Zhou, J.; Zetterberg, J.; Gustafson, J. Novel in Situ Techniques for Studies of Model Catalysts. *Acc. Chem. Res.* **2017**, *50* (9), 2326−2333.

(25) de Smit, E.; van Schooneveld, M. M.; Cinquini, F.; Bluhm, H.; Sautet, P.; de Groot, F. M. F.; Weckhuysen, B. M. On the Surface Chemistry of Iron Oxides in Reactive Gas Atmospheres. *Angew. Chem., Int. Ed.* **2011**, *50* (7), 1584−1588.

(26) Kästle, G.; Boyen, H. G.; Weigl, F.; Lengl, G.; Herzog, T.; Ziemann, P.; Riethmüller, S.; Mayer, O.; Hartmann, C.; Spatz, J. P.; Möller, M.; Ozawa, M.; Banhart, F.; Garnier, M. G.; Oelhafen, P. Micellar Nanoreactors—Preparation and Characterization of Hexag-

onally Ordered Arrays of Metallic Nanodots. *Adv. Funct. Mater.* **2003**, *13* (11), 853−861.

(27) Cuenya, B. R. Synthesis and catalytic properties of metal nanoparticles: Size, shape, support, composition, and oxidation state effects. *Thin Solid Films* **2010**, *518* (12), 3127−3150.

(28) Roldan Cuenya, B.; Behafarid, F. Nanocatalysis: size- and shape-dependent chemisorption and catalytic reactivity. *Surf. Sci. Rep.* **2015**, *70* (2), 135−187.

(29) Hoffman, A. S.; Singh, J. A.; Bent, S. F.; Bare, S. R. In situ observation of phase changes of a silica-supported cobalt catalyst for the Fischer−Tropsch process by the development of a synchrotron-compatible in situ/operando powder X-ray diffraction cell. *J. Synchrotron Radiat.* **2018**, *25* (6), 1673−1682.

(30) Ravel, B.; Newville, M. ATHENA, ARTEMIS, HEPHAESTUS: data analysis for X-ray absorption spectroscopy using IFEFFIT. *J. Synchrotron Radiat.* **2005**, *12* (4), 537−541.

(31) Grosvenor, A. P.; Kobe, B. A.; Biesinger, M. C.; McIntyre, N. S. Investigation of multiplet splitting of Fe 2p XPS spectra and bonding in iron compounds. *Surf. Interface Anal.* **2004**, *36* (12), 1564−1574.

(32) Yamashita, T.; Hayes, P. Analysis of XPS spectra of Fe^{2+} and Fe^{3+} ions in oxide materials. *Appl. Surf. Sci.* **2008**, *254* (8), 2441−2449.

(33) Mills, P.; Sullivan, J. L. A study of the core level electrons in iron and its three oxides by means of X-ray photoelectron spectroscopy. *J. Phys. D: Appl. Phys.* **1983**, *16* (5), 723−732.

(34) Jozwiak, W. K.; Kaczmarek, E.; Maniecki, T. P.; Ignaczak, W.; Maniukiewicz, W. Reduction behavior of iron oxides in hydrogen and carbon monoxide atmospheres. *Appl. Catal., A* **2007**, *326* (1), 17−27.

(35) Ding, M.; Yang, Y.; Wu, B.; Li, Y.; Wang, T.; Ma, L. Study on reduction and carburization behaviors of iron phases for iron-based Fischer−Tropsch synthesis catalyst. *Appl. Energy* **2015**, *160*, 982−989.

(36) Hong, Y.; Zhang, S.; Tao, F. F.; Wang, Y. Stabilization of Iron-Based Catalysts against Oxidation: An In Situ Ambient-Pressure X-ray Photoelectron Spectroscopy (AP-XPS) Study. *ACS Catal.* **2017**, *7* (5), 3639−3643.

(37) Zhou, X.; Mannie, G. J. A.; Yin, J.; Yu, X.; Weststrate, C. J.; Wen, X.; Wu, K.; Yang, Y.; Li, Y.; Niemantsverdriet, J. W. Iron Carbidization on Thin-Film Silica and Silicon: A Near-Ambient-Pressure X-ray Photoelectron Spectroscopy and Scanning Tunneling Microscopy Study. *ACS Catal.* **2018**, *8* (8), 7326−7333.

(38) Li, Y.; Li, Z.; Ahsen, A.; Lammich, L.; Mannie, G. J. A.; Niemantsverdriet, J. W. H.; Lauritsen, J. V. Atomically Defined Iron Carbide Surface for Fischer−Tropsch Synthesis Catalysis. *ACS Catal.* **2019**, *9* (2), 1264−1273.

(39) Heemeier, M.; Stempel, S.; Shaikhutdinov, S. K.; Libuda, J.; Bäumer, M.; Oldman, R. J.; Jackson, S. D.; Freund, H. J. On the thermal stability of metal particles supported on a thin alumina film. *Surf. Sci.* **2003**, *523* (1), 103−110.

(40) Mason, M. G. Electronic structure of supported small metal clusters. *Phys. Rev. B: Condens. Matter Mater. Phys.* **1983**, *27* (2), 748−762.

(41) Karim, W.; Kleibert, A.; Hartfelder, U.; Balan, A.; Gobrecht, J.; van Bokhoven, J. A.; Ekinci, Y. Size-dependent redox behavior of iron observed by in-situ single nanoparticle spectro-microscopy on well-defined model systems. *Sci. Rep.* **2016**, *6* (1), 18818.

(42) Wang, C.; Baer, D. R.; Amonette, J. E.; Engelhard, M. H.; Antony, J.; Qiang, Y. Morphology and Electronic Structure of the Oxide Shell on the Surface of Iron Nanoparticles. *J. Am. Chem. Soc.* **2009**, *131* (25), 8824−8832.

(43) Miller, D. J.; Biesinger, M. C.; McIntyre, N. S. Interactions of CO_2 and CO at fractional atmosphere pressures with iron and iron oxide surfaces: one possible mechanism for surface contamination? *Surf. Interface Anal.* **2002**, *33* (4), 299−305.

(44) Satthawong, R.; Koizumi, N.; Song, C.; Prasassarakich, P. Comparative Study on CO_2 Hydrogenation to Higher Hydrocarbons over Fe-Based Bimetallic Catalysts. *Top. Catal.* **2014**, *57* (6), 588−594.

(45) Yao, Y.; Hu, Y.; Scott, R. W. J. Watching Iron Nanoparticles Rust: An in Situ X-ray Absorption Spectroscopic Study. *J. Phys. Chem. C* **2014**, *118* (38), 22317−22324.

(46) Signorini, L.; Pasquini, L.; Savini, L.; Carboni, R.; Boscherini, F.; Bonetti, E.; Giglia, A.; Pedio, M.; Mahne, N.; Nannarone, S. Size-dependent oxidation in iron/iron oxide core-shell nanoparticles. *Phys. Rev. B: Condens. Matter Mater. Phys.* **2003**, *68* (19), 195423.